# Interaction of Vitamin B3 with Parent Uracil and Anticancer Uracils: A Detailed Computational Approach

F. Ravari and A. Khanmohammadi*

*Chemistry Department, Payame Noor University, Tehran 19395-4697, Iran*

*(Received 13 October 2018, Accepted 14 January 2019)*

A detailed study on the formed complexes through interaction between vitamin B3 with parent uracil and anticancer uracils is performed using M06-2X/6-311++G(d,p) and B3LYP/6-311++G(d,p) levels of theory. In the studied systems, the uracils can be placed in three preferential interaction sites (A1-A3) in the vicinity of the vitamin B3. For each uracil group, three configurations corresponding to energetic local minima are obtained. Among the various hydrogen bonding sites, the A1 region of uracils shows the strongest interactions at both levels of theory. The analyzed dimers are also stabilized by two hydrogen bonds (H-bonds). The predicted H-bonds in the formation of complexes are O···H-N and O(S)···H-O. The topological properties of the electron density distribution are also analyzed in terms of the quantum theory of "atoms in molecules" (QTAIM). Furthermore, the natural bond orbital (NBO) analysis is applied to get a more precise insight into the nature of the H-bond interactions. The calculations reveal that, in most cases, the O(S)···H-O H-bonds are stronger than the O···H-N ones. The calculated energies of highest occupied molecular orbital (HOMO) and lowest unoccupied molecular orbital (LUMO) show that charge transfer occurs within the molecules.

## INTRODUCTION

H-bonding interactions are among the key interactions characterizing the structure, functionality and dynamic processes in a large variety of systems. The investigation on H-bond is an interesting subject from theoretical and experimental viewpoints [1-7]. They are the strongest and the most common intermolecular interactions playing a very important role in nature [8-11]. These interactions frequently occur in inorganic, organic and biological chemistry [12-15]. The influence of the H-bond formation on the geometrical and topological parameters has been studied in many systems. For example, Roohi *et al.* [16] investigated the structure, stability and proton transfer in the H-bond complexes formed from the interaction between uracil and parent nitrosamine using B3LYP, B3PW91 and MP2 methods with a wide range of basis sets. Also,

Yoosefian and co-worker [17] showed the effect of various solvents on the stability order, binding energy and H-bond strength of cytosine-guanine complex using the density functional theory. In 2017, the nature and properties of H-bond interactions in adenine-thymine complex with quantum chemical calculations were analyzed by Souri et al. [18].

Uracil contains many consecutive H-bond donor and acceptor groups making it ideal for studying H-bond interactions. A variety of uracil derivatives have been reported as anti-tumor and anti-viral agents or both. Among them, 5-fluorouracil (5FU) is of particular importance. The 5FU belongs to the pyrimidine bases and is used as the most commonly cytostatic agent in oncology [19]. It is also a chemotherapeutic agent which has been used mainly for colorectal and pancreatic cancers and aggressive forms of breast cancer [20-25]. Moreover, 2-thiouracil (2TU) with a structure closely related to 5FU is studied. Baker has reported the use of thiouracil for the treatment of hyperthyroidism [26,27]. Furthermore, thiouracils are

_____
*Corresponding author. E-mail: az_khanmohammadi@yahoo.com

known as effective neoplastigen, tumorigen, carcinogen and tetragen agents controlling the virus and bacterial growth, inhibit kidney stone formation and possess antidote properties for mercury poisoning [26].

Vitamin B3 is one of 8 B vitamins. It is an organic compound and an essential human nutrient. Vitamin B3, also known as niacin or nicotinic acid is a water-soluble vitamin that has the formula $C_6H_5NO_2$. It belongs to the group of pyridinecarboxylic acid. In other words, it is a derivative of pyridine, with a carboxyl group (COOH) at the 3-position. An absence of vitamin B3 causes the deficiency disease pellagra, dementia, diarrhea, and skin problems such as dermatitis [28,29]. The liver can synthesize vitamin B3 from the essential amino acid of tryptophan, which is found in protein-containing foods [30].

There are different interactions between vitamins and drugs leading to the positive or negative effects on health which must not be overlooked. For instance, the drug isoniazid may cause vitamin B3 deficiency disease as it reduces the conversion of tryptophan to vitamin B3. Furthermore, vitamin B3 may reduce the toxic side effects on heart tissue of the anticancer drug adriamycin without reducing its effectiveness in the treatment of cancer. It is also well known as an inhibitor of metastasis in human breast carcinoma cells [29]. In addition, it may enhance the effectiveness of anticonvulsant drugs such as phenobarbital. In the present study, molecular modeling on the formed complexes between VB3 and uracil shows the full ability of the drugs for participating in the formation of a stable intercalation site. It is completed that the binding energy and the electrostatic interaction contribute to the stability of these complexes. H-bond interactions between or within the molecules leads to the stable compounds Because of the importance of vitamin B3 in various food categories, the interaction between drugs and this vitamin and their corresponding effects on their properties are of a great importance. Furthermore, these complexes can be considered as model systems for understanding the H-bonding interactions in biomolecules.

The main goal of this study is to find the complexes formed from interaction between the vitamin B3 (VB3) with the parent uracil (U) and anticancer uracils of 5-fluorouracil (5FU) and 2-thiouracil (2TU). The geometrical parameters, binding energies and topological properties are examined to gain further insight into the effect of mentioned interactions on H-bond strength. In addition, the AIM and NBO analyses are employed to elucidate the nature of intermolecular H-bond interactions. The frontier orbital analysis is also carried out to indicate the remarkable role of HOMO-LUMO charge transfer in stability and chemical reactivity of the complexes. Finally, several correlations between topological, geometrical and energetic parameters are found.

## THEORETICAL METHOD

All calculations are carried out using the Gaussian 03 package [31]. Initially geometries of the isolated monomers and molecular complexes are optimized within the framework of density functional theory (M06-2X and B3LYP) at the level of 6-311++G(d,p). Selection of basis set is done based on considering both polarization function and diffuse function to give more accurate results. The vibrational frequencies are used to characterize stationary points and calculation of zero-point vibrational energy (ZPVE). The computations demonstrate that the studied complexes are in global minima and no imaginary frequency is obtained for such structures. The counterpoise procedure (CP) [32] is also applied to correct basis set superposition error (BSSE) in the calculation of binding energies. The binding energies ($\Delta E$) are obtained as the difference between the energy of the complex (AB) and the combination of the energies of the isolated species A and B [33,34],

$$\Delta E = E_{AB} - (E_A + E_B) \quad\quad\quad (1)$$

In this exploration, the values of the intermolecular H-bond energies are calculated approximately by the Espinosa and Molins methods [35]. To get more information about the nature of the H-bond interactions, a topological analysis is carried out to calculate the electron density ($\rho$) and its second derivative ($\nabla^2\rho$) at bond critical point (BCP) by the atoms in molecules (AIM) method [36]. The AIM analysis is performed using the AIM2000 program [37] on the obtained wave functions at the M06-2X/6-311++G(d,p) and B3LYP/6-311++G(d,p) levels of theory. Also, the natural bond orbital (NBO) analysis is carried out on the optimized
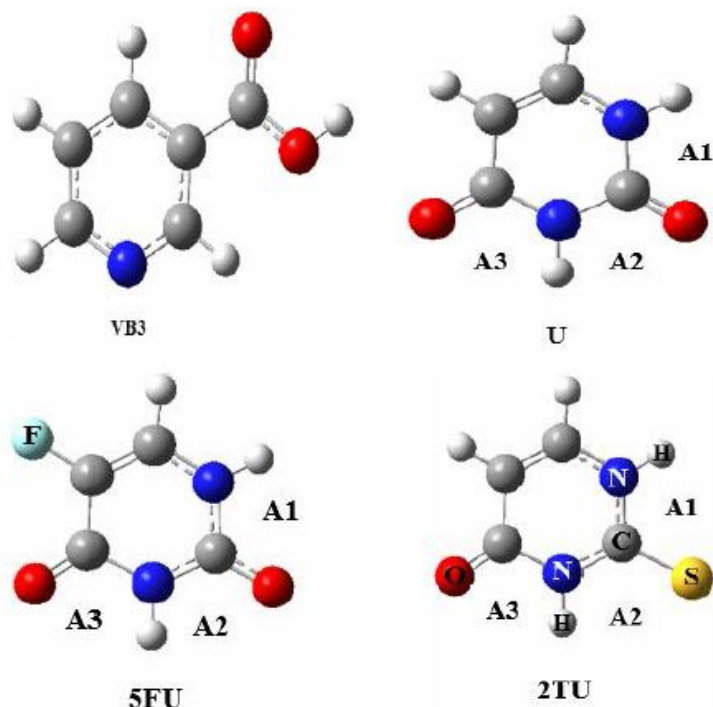
**Fig. 1.** Structures of vitamin B3 (VB3), parent uracil (U) and anticancer uracils of 5-fluorouracil (5FU) and 2-thiouracil (2TU).

structures with NBO program (version 3.1) included in Gaussian 03 package [38]. Furthermore, the molecular orbital (MO) calculations such as the highest occupied MO (HOMO) and lowest unoccupied MO (LUMO) are performed on all complexes with the same levels of DFT theory. The chemical hardness ($\eta$) and electronic chemical potential ($\mu$) are calculated using the HOMO and LUMO energies.

## RESULTS AND DISCUSSION

### Molecular Geometries

Figure 1 shows that uracil can be placed in three preferential interaction sites (A1-A3) in the vicinity of the vitamin B3. For each uracil group (U, 5FU and 2TU), three configurations corresponding to energetic local minima are obtained. The complexes formed between the vitamin B3 with the anticancer uracils of 5-fluorouracil, 2-thiouracil and parent uracil are depicted in Fig. 2. Numbering system for the various uracils in vicinity of the vitamin B3 including complexes of the uracil and vitamin B3 (U-VB), the

5-fluorouracil and vitamin B3 (FU-VB) and 2-thiouracil and vitamin B3 (TU-VB) is represented in this figure. The corresponding structures of each complex are shown through numerical numbering from 1 to 3. Based on our numbering system, the U-VB1, U-VB2 and U-VB3 describe first, second and third configurations of complex U-VB, respectively. As shown in Fig. 2, the VB3 and uracils can act simultaneously as proton donors and proton acceptors. Two different intermolecular interactions are predicted that participate in the formation of complexes, namely: conventional $O_{VB}\cdots H\text{-}N_U$ and $O(S)_U\cdots H\text{-}O_{VB}$ H-bonds. Therefore, all systems analyzed here are coupled through two H-bonds. Result of computations also shows that all of the complexes are completely planar or without partial pyramidal character at the internal nitrogen atoms of uracils. Geometrical parameters also confirm the planarity of complexes according to their dihedral angles. The results show that the dihedral angles in all of the complexes are 180° which can be a reason for their planarity. It can be also stated that the planarity of the studied complexes is due to the extra electron resonance between the corresponding
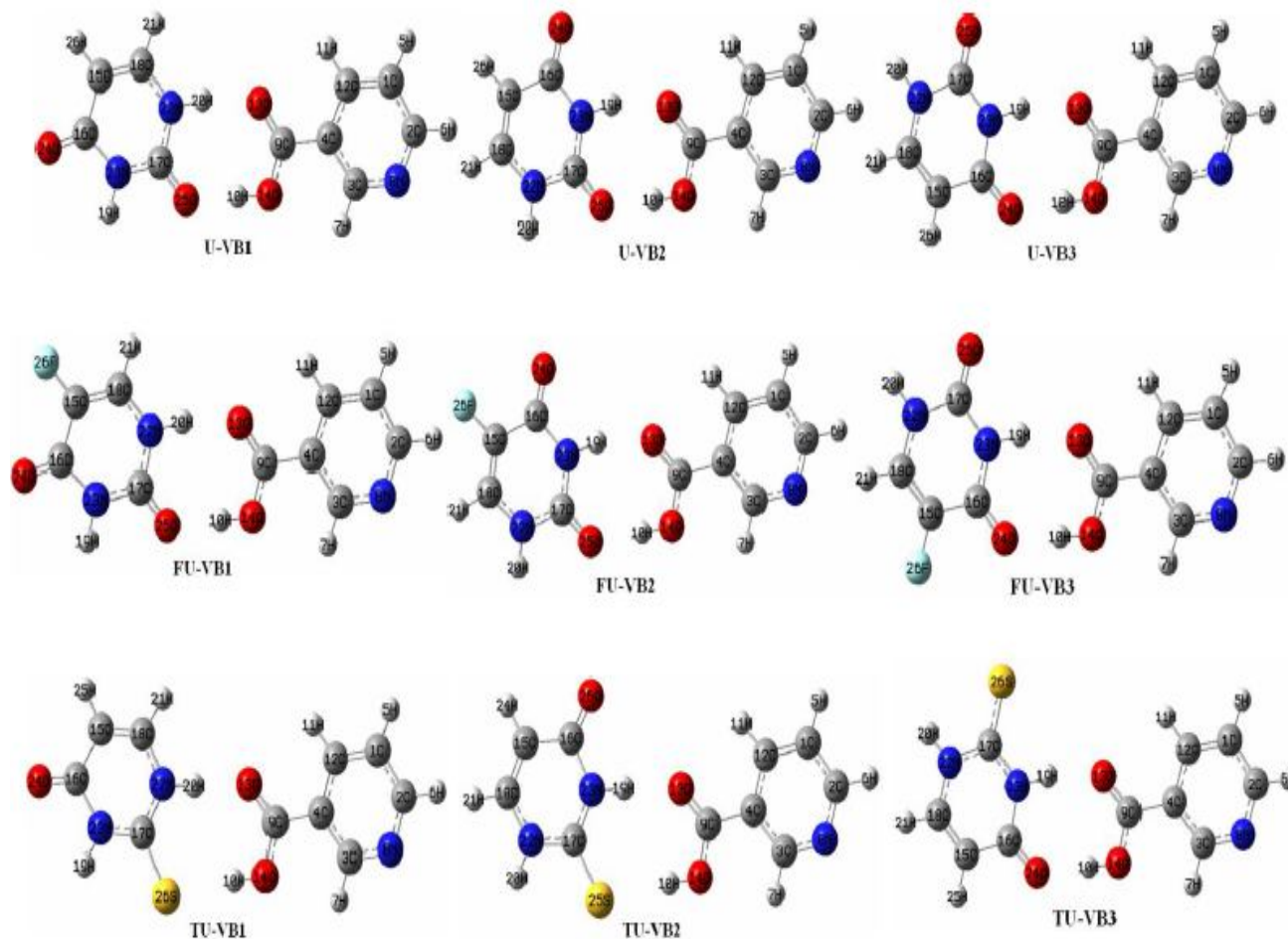
**Fig. 2.** Numbering system for the A1-A3 regions of uracil in vicinity of the vitamin B3, including complexes of uracil and vitamin B3 (U-VB), 5-fluorouracil and vitamin B3 (FU-VB), and 2-thiouracil and vitamin B3 (TU-VB).

atoms. There is the long conjugation between different atoms in the related complexes. The long resonance will be formed as O24···C16···C15···C18···N22 atoms (uracils) and O13···C9···C4···C3···N8 atoms (VB3) in all of the complexes. As can be seen, these resonance structures show that all of the complexes have one terminal nitrogen atom and the other terminal donating group is oxygen atom. In these complexes, the terminal nitrogen N atom contributes to extra resonance. Due to the more electron-donating character of nitrogen in comparison with the oxygen, it is assumed to be the reason for the stability of these complexes. The theoretical results reveal that complexes U and FU having two carbonyl functional groups in a trans position

relative to each other are more stable than TU. The more stability of complexes U and FU with respect to complexes TU can be attributed to extra-resonance structure of complexes U and FU in comparison to complexes TU. Donation of electrons from nitrogen N23 atom to the corresponding π* of carbonyl group (C16=O24 double bond) can be a reason for more stability of these complexes (data not reported). Complexes TU containing weaker carbon-sulfur double bond (C=S) are the most unstable ones. This can be due to the lack of extra resonance structure in these complexes.

It is obvious from Fig. 2 that, in most cases, the H-bonds of the formed complexes are $O_{VB}$···$H-N_U$ and

$O_U \cdots H\text{-}O_{VB}$, whereas they are different for TU-VB1 and TU-VB2 complexes ($O_{VB} \cdots H\text{-}N_U$ and $S_U \cdots H\text{-}O_{VB}$). The electronic properties of this class of complexes depend on the strength of the donor and acceptor groups and the length of the generated bridges between monomers. In TU-VB1 and TU-VB2 complexes, it is revealed that sulfur atom is a very poor H-bond acceptor [39]. Sulfur-containing H-bonds are longer than those formed between nitrogen or oxygen atoms because of the larger size and more diffuse electron cloud of sulfur. On the other hand, the nonbonding electron pairs of sulfur atom are nearly perpendicular to the ring plane, so, when are served as H-bonds acceptor, they are prone to form weak interactions. Platts *et al.* [40,39] investigated the directionality of H-bonds to sulfur and oxygen. They indicated that H-bond formation to oxygen is driven by charge-charge interactions, whereas, in sulfur case, the stabilization arises principally from the interaction of the charge on the acidic hydrogen with the dipole and quadrupoles of sulfur.

In this study, we have also investigated the H-bond distances of the formed complexes as one of the indicators of H-bond strength [41]. The geometrical parameters of H-bond for all of the complexes using M06-2X/6-311++G(d,p) level of theory are listed in Table S1 (supplementary material). Similar data for bond lengths and bond angles are obtained when B3LYP/6-311++G(d,p) (Table S2) is used instead of M06-2X/6-311++G(d,p) method. As observed in these tables, the shortest H-bond contact ($O(S)_U \cdots H_{VB}$) are observed for $O(S)_U \cdots H\text{-}O_{VB}$ H-bonds (except for TU-VB1 and TU-VB2 complexes), while the longest one ($O_{VB} \cdots H_U$) corresponds to $O_{VB} \cdots H\text{-}N_U$ H-bonds. Furthermore, it can be stated that $O\text{-}H_{(VB)}$ and $N\text{-}H_{(U)}$ distances involved in H-bond increase in complexes in comparison with their monomers (data not reported). Thus, it can be concluded that the increment of $O\text{-}H_{(VB)}$ bond length value (due to $O(S)_U \cdots H\text{-}O_{VB}$ H-bonds) is accompanied by increasing H-bond strength in the related complexes. These results clearly show that H-bond for the $O(S)_U \cdots H\text{-}O_{VB}$ interactions is stronger than that for the $O_{VB} \cdots H\text{-}N_U$ ones. The $O(S)_U \cdots H\text{-}O_{VB}$ and $O_{VB} \cdots H\text{-}N_U$ angles can also be an explanation for the H-bond strength. It is well known that the closer to the angle of 180°, the stronger is the H-bond. According to Tables S1 and S2, the intermolecular $O(S)_U \cdots H\text{-}O_{VB}$ angles are clearly larger than

the $O_{VB} \cdots H\text{-}N_U$ ones. In fact, higher angle value among $O(S)_U$, $H_{VB}$ and $O_{VB}$ atoms make stronger H-bonding, because H-bonding is dependent on both bond angle and bond length in addition to the nature of electronegative atoms. In the $O(S)_U \cdots H\text{-}O_{VB}$, the formation of H-bond arises from movement of proton between two oxygen (or sulfur) and oxygen atoms, but in the $O_{VB} \cdots H\text{-}N_U$ such H-bond arises from movement of proton between nitrogen and oxygen atoms. The more electronegativity of oxygen atom relative to the nitrogen analogue makes it to diminish the O-H bond strength. So, proton can be easily detached by another oxygen atom compared to N-H bond.

**Energies**

In this investigation, the approximate values of the intermolecular H-bond energies are calculated by the Espinosa and Molins methods [35]. Calculated M06-2X/6-311++G(d,p) and B3LYP/6-311++G(d,p) H-bond energies ($E_{HB}$) for all of the related complexes are demonstrated in Table 1. For a stronger H-bond, this kind of complexation usually leads to (i) the elongation of the N(O)-H bonds length as proton donor, (ii) the shortening of the $O(S) \cdots H$ distances as proton acceptor, and (iii) the increment of the $O(S) \cdots H\text{-}O$ and $O \cdots H\text{-}N$ angles. Tables S1 and S2 show that, in most cases, the $O_{VB} \cdots H_U$ and $O(S)_U \cdots H_{VB}$ distances corresponding to the $O_{VB} \cdots H\text{-}N_U$ and $O(S)_U \cdots H\text{-}O_{VB}$ H-bonds for the U-VB1, FU-VB1 and TU-VB1 planar dimers are the lowest, whereas the highest ones belong to the U-VB2, FU-VB2 and TU-VB2 complexes; hence, the strength of H-bond is maximum for the former dimers with respect to the latter. It can be concluded that the estimated results at the H-bond energies are completely in accordance with the results obtained in its geometrical parameters.

Values of the calculated binding energies without and with the ZPE correction ($\Delta E_{NO\text{-}ZPE}$ and $\Delta E_{ZPE}$) along with both the BSSE and ZPE contributions ($\Delta E_{BSSE}$) for all structures are calculated at both the M06-2X/6-311++G(d,p) and B3LYP/6-311++G(d,p) levels of theory and are demonstrated in Table 1. It is worth mentioning that the absolute values of binding energies achieved using M06-2X/6-311++G(d,p) are greater than those obtained at the B3LYP/6-311++G(d,p) level of theory (see Table 1). The calculated binding energies in the H-bond formation process

**Table 1.** Calculated Binding Energies without and with the ZPE Correction ($\Delta E_{NO\text{-}ZPE}$ and $\Delta E_{ZPE}$) along with both the BSSE and ZPE Contributions ($\Delta E_{BSSE}$), the H-bond Energies ($E_{HB}$) and the Changes in Thermodynamic Functions (in Terms of kJ mol$^{-1}$) upon Complex Formation

| Method | | $\Delta E_{No\text{-}ZPE}$ | $\Delta E_{ZPE}$ | $\Delta E_{BSSE}$ | $\Delta G$ | $\Delta H$ | $E_{HB}$ ($O_{VB}\cdots H\text{-}N_U$) | $E_{HB}$ ($O(S)_U\cdots H\text{-}O_{VB}$) |
|---|---|---|---|---|---|---|---|---|
| M06-2X | U-VB1 | -74.74 | -71.88 | -68.24 | -22.30 | -66.82 | -38.01 | -60.95 |
| | U-VB2 | -62.82 | -60.61 | -56.95 | -15.23 | -54.85 | -31.75 | -51.86 |
| | U-VB3 | -65.67 | -62.83 | -59.44 | -14.09 | -57.74 | -33.64 | -57.14 |
| | FU-VB1 | -74.95 | -72.01 | -68.32 | -22.45 | -66.84 | -41.50 | -57.42 |
| | FU-VB2 | -64.56 | -61.43 | -57.66 | -12.76 | -55.76 | -34.05 | -51.01 |
| | FU-VB3 | -64.11 | -61.29 | -57.74 | -12.01 | -55.98 | -33.40 | -51.69 |
| | TU-VB1 | -65.98 | -64.62 | -61.55 | -18.94 | -59.33 | -43.17 | -24.18 |
| | TU-VB2 | -52.97 | -51.57 | -48.44 | -7.76 | -45.97 | -36.31 | -21.86 |
| | TU-VB3 | -63.82 | -61.61 | -58.08 | -13.66 | -56.13 | -35.83 | -51.91 |
| | | | | | | | | |
| B3LYP | U-VB1 | -67.78 | -63.41 | -60.13 | -13.54 | -58.99 | -40.89 | -59.90 |
| | U-VB2 | -54.96 | -50.92 | -47.60 | -1.99 | -46.04 | -31.58 | -53.74 |
| | U-VB3 | -58.82 | -54.80 | -51.71 | -5.40 | -50.35 | -34.19 | -59.69 |
| | FU-VB1 | -68.29 | -64.10 | -60.76 | -13.99 | -59.59 | -43.78 | -57.82 |
| | FU-VB2 | -56. 35 | -52.43 | -49.00 | -2.96 | -47.43 | -35.07 | -52.30 |
| | FU-VB3 | -57.20 | -53.30 | -50.02 | -3.88 | -48.51 | -36.02 | -53.43 |
| | TU-VB1 | -59.23 | -56.28 | -53.48 | -8.06 | -51.75 | -43.78 | -25.50 |
| | TU-VB2 | -44.51 | -41.89 | -39.02 | 5.41 | -36.92 | -35.35 | -22.72 |
| | TU-VB3 | -56.39 | -52.55 | -49.30 | -2.99 | -47.81 | -35.18 | -56.63 |

are defined as the energy difference between the optimized complexes and the sum of the individual monomers. The binding strength of the studied complexes is dependent on the interaction site. In the investigated species, it can be seen that the binding energy between the monomers will depend not only on the basicity of the acceptor groups but also on the acidity of the donor groups. The basicity of the two oxygen atoms and the acidity of the two NH bonds of uracil have been discussed in several works, and it has been suggested that both carbonyl groups are comparable in their acceptor strength [42-45]. In 1998, Nguyen *et al.* [45] investigated the protonation and deprotonation energies of uracil for the uracil-water complex. From obtained results, they found that the more acidic and less basic sites participate to form the most stable complex. In this study, based on calculated proton affinities (PA) [45], the most

basic site of uracil (O24 at the C15 side) belongs to U-VB3, whereas the PA of the O25 atom at both N22 and N23 sides are sensibly lower (related to U-VB1 and U-VB2). Therefore, it can be stated that the two lone pairs of the O24 and O25 atoms are not equivalent. On the other hand, the acidity of the N22-H20 bond (U-VB1) is higher than that of the N23-H19 bond (U-VB2 and U-VB3). This result has been explored by a deprotonation energy [45]. The reason for this high acidity is probably a strong delocalization in the O24=C16-C15=C18-N22 part of the molecule. According to these results, the A1 region of uracil should be the most stable and the A2 and A3 regions of uracil should have less stability than A1 region. In other words, the most stable H-bond can be formed at the site characterized by the lowest PA and the highest acidity.

It is obvious that the achieved results in this study confirm the above-mentioned consequences. For each uracil group (U, 5FU and 2TU), the relative stability order based on the calculated binding energies is as follows:

FU-VB1 > U-VB1 > TU-VB1 > U-VB3 > TU-VB3 > FU-VB3 > FU-VB2 > U-VB2 > TU-VB2
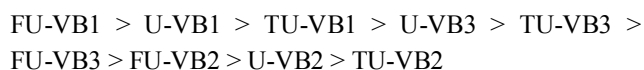
As can be seen, among the various H-bonding sites, the A1 region of uracils shows the strongest interactions, whereas the weakest ones belong to the A2 region (see Table 1). The binding energies are also obtained at the B3LYP/6-311++G(d,p) level of theory for stability comparison of the related complexes. The results show that the order of stabilities, except one case, does not change. For the selected species, the contribution of ZPE in binding energies is obtained by both the B3LYP and M06-2X methods. It is found out that the ZPE correction could not change the energy orders. Therefore, it is an insensitive parameter. The counterpoise procedure (CP) [32] is also applied to correct basis set superposition error (BSSE) in the calculation of binding energies. After BSSE correction, it seems that the complexes U-VB1, FU-VB1 and TU-VB1 are more stable than the others. Therefore, the predicted relative stabilities with the BSSE correction and without it are equal for all complexes and does not change (see Table 1). The thermodynamic properties such as enthalpy ($\Delta H$) and Gibbs free energy ($\Delta G$) for all complexes are also calculated with both the M06-2X and B3LYP methods and

the results are listed in Table 1. The obtained free energy values show that the U-VB1, FU-VB1 and TU-VB1 complexes have the strongest interactions at the both levels of theory. Therefore, selected species are the most stable complexes with respect to the other ones. The same results will be seen if one considers the achieved values for $\Delta E_{NO-ZPE}$, $\Delta E_{ZPE}$ and $\Delta H$. Therefore, the interaction site and the extra resonance structure between atoms can cause more stability of these complexes relative to others.

For the purpose of comparison, the optimization on the FU-VB1 complex is also estimated through M06-2X/6-311+G and M06-2X/6-311++G methods (see Table S3). The results reveal that all respective bond lengths obtained by 6-311+G and 6-311++G (basis sets without polarization function) are almost the same; however, when the polarization function is included in the basis set, corresponding bond lengths are increased in O(S)···H distances and are decreased in N(O)-H bonds, for both levels of theory. In fact, the N(O)-H bond lengths vary slightly for the three basis sets at the DFT levels of theory. Inclusion of polarization functions has changed the O(S)···H distances considerably. Table S3 also indicates the H-bonds and binding energies of the FU-VB1 complex using different basis sets and levels of theory. It is interesting to note that the absolute values obtained from the 6-311+G and 6-311++G basis sets are more than those achieved using 6-311++G(d,p) basis functions. This shows that the energy values change remarkably when the basis function with diffuse and polarization function are used at the DFT level of theory. The calculated stretching frequencies are also found to be the largest for the 6-311+G and 6-311++G basis sets and the smallest for 6-311++G(d,p) basis function at the both levels of theory. Based on the results, it can be concluded that the level of theory, basis set size and inclusion of diffusion and polarization functions have an effective contribution in H-bonding.

Results also indicate an excellent linear relationship between the sum of H-bond formation energies ($\Sigma E_{HB}$) and the sum of the O(S)$_U$···H$_{VB}$ and O$_{VB}$···H$_U$ distances ($\Sigma d_{O(S)···H}$) involved in O$_{VB}$···H-N$_U$ and O(S)$_U$···H-O$_{VB}$ H-bonds, with an equation as: $\Sigma E_{HB} = 56.128\ (\Sigma d_{O(S)···H}) - 288.13$. The correlation coefficient (R) is equal to 0.955. This correlation shows that the O(S)$_U$···H$_{VB}$ and O$_{VB}$···H$_U$ distances reduce as the H-bonds strength enhance. There is also a relatively

good correlation between the values of binding energy ($\Delta E$) versus the sum of the N-H and O-H contacts ($\Sigma d_{N(O)-H}$) involved in H-bonds with the correlation coefficient of 0.834, according to the equation shown bellow;

$$\Delta E = -2213.5 \ (\Sigma d_{N(O)-H}) + 4406.5$$

It is obvious that the O-H$_{(VB)}$ proton donating bond due to H-bond formation is usually elongated and this lengthening is greater for stronger H-bonds. Our theoretical results reveal that the maximum and minimum of the $\Sigma d_{N(O)-H}$ contacts (2.021 Å) and the $\Sigma d_{O(S)\cdots H}$ distances (3.463 Å) correspond to the FU-VB1 complex, respectively. This result is also in agreement with the greatest absolute value of $\Delta E$ (-68.32 kJ mol$^{-1}$) for this complex. These results are also confirmed at the B3LYP/6-311++G(d,p) level of theory.

Dipole moment ($\mu$) is also a quantity for describing the studied systems. In this study, the molecular dipole moments of the analyzed complexes and their monomers are calculated using DFT methods (see Tables S1 and S2). The results show that the predicted dipole moment of the VB3 is 0.68 D, which is found to be much smaller than the uracil monomers (U = 4.54, 5FU = 4.14 and 2TU = 4.74). This indicates that when the VB3 monomer enters into the different sites of the drug, the net dipole moment of the molecule increases and the orientation of the dipole moment vector also changes. The obtained results also demonstrate that the calculated dipole moments are quite large for these systems (see Tables S1 and S2). The large dipole moments exhibit the high reactivity of molecules. This enhancement of dipole moment is also due to the charge redistribution and migration of charges from one region of molecule to the other region leading to the intermolecular interactions between the VB3 and uracils. In this study, the hydrogen atoms show the highest positive charges, due to their bonding to the oxygen and nitrogen atoms with high electronegativity. Existence of electronegative elements in these monomers facilitates their self-interactions through H-bond formation with the hydrogen atoms. Therefore, results reveal a greater tendency of VB3 to form H-bond as donor with respect to the parent uracil and uracils of 5FU and 2TU.

**Vibrational Frequencies**

In continuation of our studies for a better elucidation of H-bond strength, vibrational frequencies for all complexes are calculated at the M06-2X/6-311++G(d,p) (Table S1) and B3LYP/6-311++G(d,p) (Table S2) levels of theory. It is well established that the larger the frequency shift, the more stable is the complex. So, in this paper, we have shown some important frequency shifts in order to investigate the relative stabilities of the complexes. As shown in Tables S1 and S2, the frequency shifts ($\Delta \upsilon$) are defined as the difference between the frequency of the certain vibrational mode in complex and in isolated monomer, and can be expressed as:

$$\Delta \upsilon = \upsilon_{complex} - \upsilon_{monomer}.$$

The obtained computations predict that the vibrational frequencies of N-H and O-H bonds involved in H-bonding are red-shifted. Result of calculations also shows that the O-H vibrational frequencies appear a larger red shift in the O(S)$_U \cdots$H-O$_{VB}$ H-bonds, whereas a smaller red shift in the N-H vibrational frequencies observes for the O$_{VB} \cdots$H-N$_U$ H-bonds. Our theoretical results based on the sum of N–H and O-H vibrational frequencies values show that the U-VB1, FU-VB1 and TU-VB1 complexes have the greatest red shift, whereas the least red shift belongs to the U-VB2, FU-VB2 and TU-VB2 complexes. As going from Table S1, the trend in the values of binding energies is identical with the changes of sum of vibrational frequencies. In other words, amount of red shift in the most stable complexes is greater than other ones. Similar results are also obtained for the studied complexes at the B3LYP/6-311++G(d,p) level of theory (see Table S2). There is a relatively good linear relationship between the sum of N(O)-H stretching frequencies ($\Sigma \Delta \upsilon$) involved in O$_{VB} \cdots$H-N$_U$ and O(S)$_U \cdots$H-O$_{VB}$ H-bonds and the binding energies ($\Delta E$). The correlation coefficient is equal to 0.885. This dependency is shown in Fig. 3. The obtained results in this study also show that the B3LYP method creates a better correlation between the $\Sigma \Delta \upsilon$ and $\Delta E$ values in comparison with the M06-2X method (see Fig. S1). This correlation confirms that the red-shifted values can also affect the strength of H-bond interactions in the corresponding complexes. Thus, the stretching frequencies may be a useful parameter for
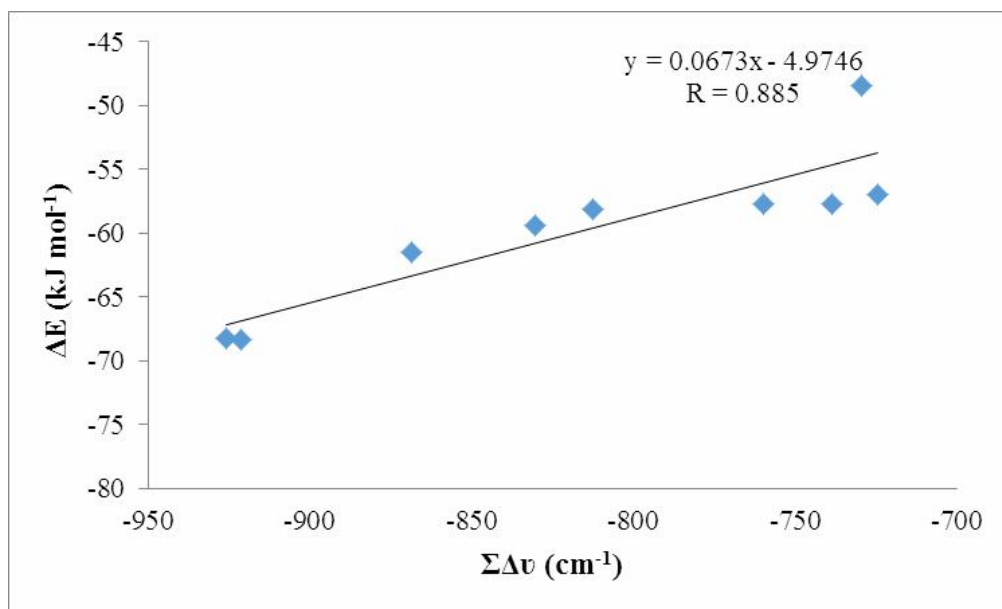
**Fig. 3.** Correlation between the binding energies ($\Delta E$) and sum of the N-H and O-H stretching frequencies ($\Sigma\Delta\upsilon$) at the M06-2X/6-311++G(d,p) level of theory.

describing the strength of these interactions.

**AIM Analysis**

In addition to the geometric and energetic analyses, the theory of atoms in molecules is also applied in the analysis of H-bonds. The parameters derived from this theory, such as the electron density, $\rho(r)$, its Laplacian, $\nabla^2\rho(r)$ and the total electron energy density, (H) [the sum of the electron energy densities of kinetic (G) and potential (V)] indicate the type of interaction. The contour map and the AIM molecular graph including bond paths (BPs) and bond critical points (BCPs) of the FU-VB1 complex are demonstrated in Fig. 4. As shown in this figure, the selected complex is characterized by an eight-membered ring formed through a pair of two parallel intermolecular H-bonds in $O(S)_U\cdots H-O_{VB}$ and $O_{VB}\cdots H-N_U$ distances.

The calculated topological parameters of the analyzed complexes at the M06-2X/6-311++G(d,p) level of theory are given in Table 2. The obtained results show that the greatest electron densities observe for the $O(S)_U\cdots H-O_{VB}$ H-bonds (except for TU-VB1 and TU-VB2 complexes), while the smallest ones belong to the $O_{VB}\cdots H-N_U$ H-bonds. Calculations show the same results for the values of $\nabla^2\rho(r)$ at the BCPs of the related complexes. It is also obvious from

Tables 1 and 2 that the increasing electron density at BCP is accompanied by increasing H-bond strength. Therefore, the AIM results confirm that the $O(S)_U\cdots H-O_{VB}$ H-bonds are stronger than $O_{VB}\cdots H-N_U$ ones. These considerations on the strength of H-bonds are also supported by the $O(S)_U\cdots H-O_{VB}$ and $O_{VB}\cdots H-N_U$ distances.

The results also indicate that, in most cases, the maximum $\rho_{BCP}$ values corresponding to the $O_{VB}\cdots H-N_U$ and $O(S)_U\cdots H-O_{VB}$ H-bonds are observed in the U-VB1, FU-VB1 and TU-VB1 complexes, whereas the minimum $\rho_{BCP}$ values are obtained for U-VB2, FU-VB2 and TU-VB2 complexes. Furthermore, among all complexes, the highest sum of $\rho_{BCP}$ values involved in H-bonds, and the maximum absolute value of binding energy belong to the most stable complex FU-VB1 (see Tables 1 and 2). As a result, the H-bond in FU-VB1 is stronger than the other complexes. Based on the results, it can be concluded that the trend in $\rho_{BCP}$ and $|\Delta E|$ values is identical with $|E_{HB}|$ values (due to $O_{VB}\cdots H-N_U$ H-bonds). This trend is reversed for H-bonding distances.

According to Rozas *et al*. [46], the character of H-bond interaction can be classified as function of the total electron energy density H(r) with its Laplacian at the BCP, $\nabla^2\rho(r)$. It means that for strong H-bonds ($\nabla^2\rho(r) < 0$ and H(r) < 0),
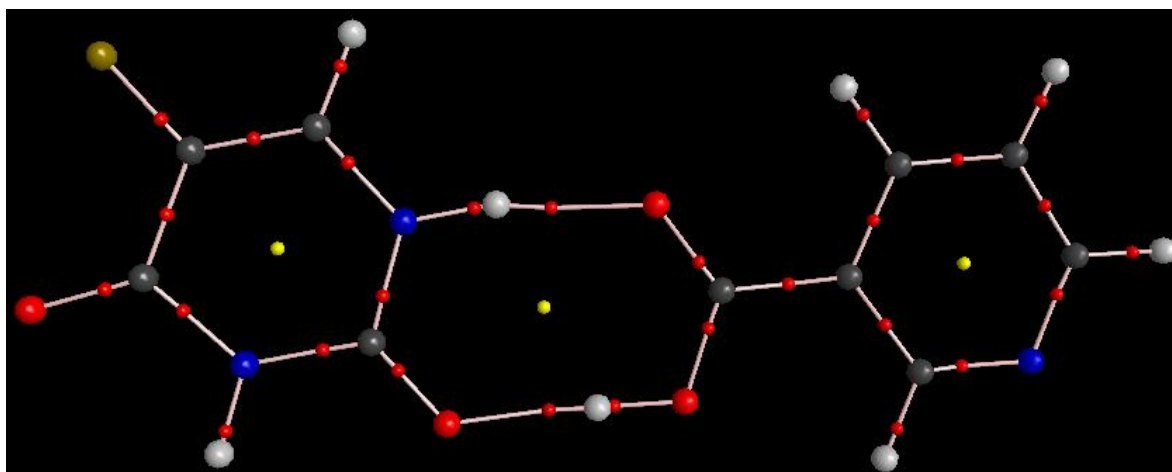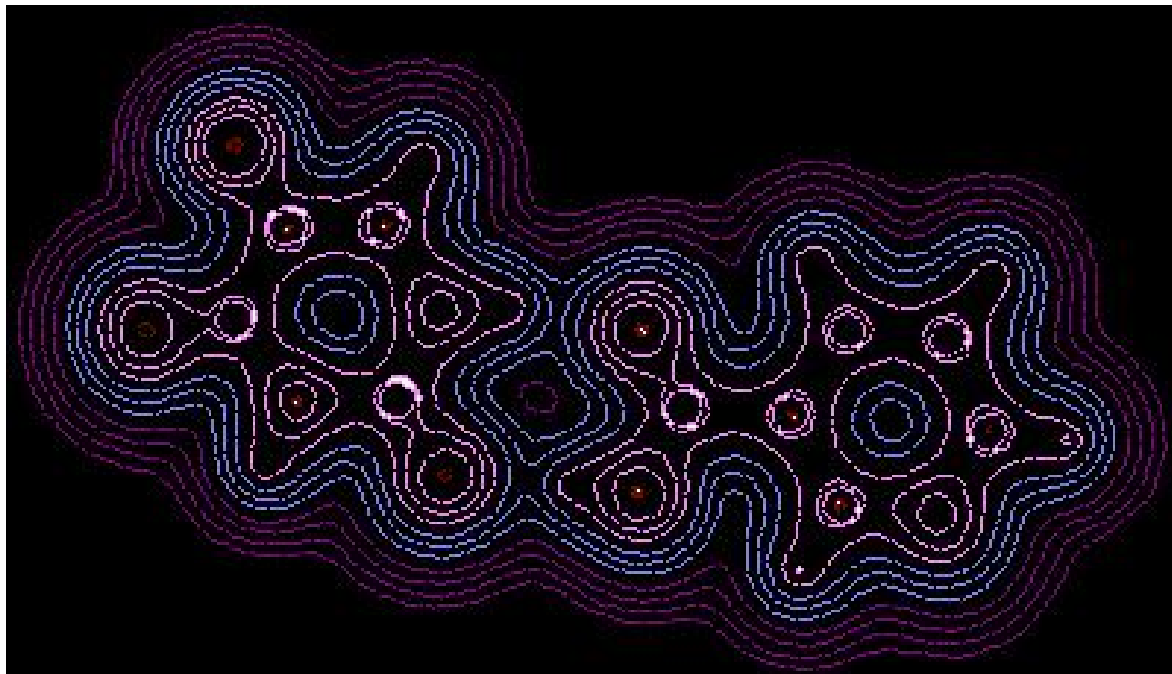
**Fig. 4.** Schematic representation of distribution of critical points in the FU-VB1 complex. Small red spheres, small yellow spheres, and lines represent bond critical points (BCPs), ring critical points (RCPs), and bond paths, respectively.

the covalent character is established, for medium strength H-bonds ($\nabla^2\rho(r) > 0$ and $H(r) < 0$), its partly covalent character is defined, and weak H-bonds ($\nabla^2\rho(r) > 0$ and $H(r) > 0$) are mainly electrostatic [47]. The obtained results at the M06-2X/6-311++G(d,p) level show that the $O_{VB}\cdots H\text{-}N_U$

H-bond in the TU-VB1 complex is the partly covalent (medium H-bonds), while the remains are noncovalent (weak H-bonds). When B3LYP/6-311++G(d,p) is used as a method of calculation, the outcome demonstrates that the $O_{VB}\cdots H\text{-}N_U$ H-bonds are partly covalent for the U-VB1,

**Table 2.** Some Topological Parameters (in a.u.) Calculated at the M06-2X/6-311++G(d,p) Level of Theory

| | $O_{VB}{\cdots}H{-}N_U$ | | | $O(S)_U{\cdots}H{-}O_{VB}$ | | |
|---|---|---|---|---|---|---|
| | $\rho_{O{\cdots}H}$ | $\nabla^2\rho_{O{\cdots}H}$ | H(r) | $\rho_{O(S){\cdots}H}$ | $\nabla^2\rho_{O(S){\cdots}H}$ | H(r) |
| U-VB1 | 0.0323 | 0.1223 | 0.0008 | 0.0461 | 0.1483 | -0.0047 |
| U-VB2 | 0.0281 | 0.1116 | 0.0019 | 0.0407 | 0.1425 | -0.0019 |
| U-VB3 | 0.0294 | 0.1148 | 0.0015 | 0.0439 | 0.1456 | -0.0036 |
| FU-VB1 | 0.0345 | 0.1280 | 0.0002 | 0.0441 | 0.1452 | -0.0037 |
| FU-VB2 | 0.0296 | 0.1160 | 0.0015 | 0.0401 | 0.1421 | -0.0017 |
| FU-VB3 | 0.0292 | 0.1143 | 0.0016 | 0.0406 | 0.1420 | -0.0019 |
| TU-VB1 | 0.0354 | 0.1310 | -7E-05 | 0.0269 | 0.0546 | -0.0024 |
| TU-VB2 | 0.0310 | 0.1214 | 0.0013 | 0.0248 | 0.0546 | -0.0015 |
| TU-VB3 | 0.0308 | 0.1194 | 0.0013 | 0.0408 | 0.1414 | -0.0021 |

FU-VB1 and TU-VB1 complexes. The calculations also reveal that for all of the $O(S)_U{\cdots}H{-}O_{VB}$ interactions the total electron energy density at the corresponding BCPs is negative. This indicates that such interactions are the partly covalent in nature (medium H-bonds) at both levels of theory. Table S4 shows the topological parameters of the analyzed complexes calculated at the B3LYP/6-311++G(d,p) level of theory. The results achieved show that the agreement between both M06-2X and B3LYP methods is relatively satisfactory.

In this study, a series of dependences are found between the geometrical, topological and energetic parameters. As shown in Fig. 5 (M06-2X/6-311++G(d,p) level) and Fig. S2 (B3LYP/6-311++G(d,p) level), there is an excellent linear correlation between the sum of electron densities ($\sum\rho_{BCP}$) and its Laplacian ($\sum\nabla^2\rho_{BCP}$) at the $O(S)_U{\cdots}H{-}O_{VB}$ and $O_{VB}{\cdots}H{-}N_U$ H-bonds with the sum of H-bond energies ($\Sigma E_{HB}$). Our theoretical results also show a remarkable correlation between the electron density at BCP of related to every H-bond in the studied complexes and their corresponding H-bond lengths. The following equations illustrate these relationships:

$\ln(\rho O_{VB}{\cdots}H_U) = -2.5517\ (dO_{VB}{\cdots}H_U) + 1.1875,$
R = 0.989

$\ln(\rho O(S)_U{\cdots}H_{VB}) = -0.9037\ (dO(S)_U{\cdots}H_{VB}) - 1.6361,$
R = 0.987

It is clear that the electron densities increase exponentially as $O(S){\cdots}H$ distances decrease. From the obtained results, it can be concluded that the shorter distance is attributed to the greater strength of H-bond and the higher electron density at $O(S){\cdots}H$ contacts. These results indicate that the geometrical and topological parameters could be very useful to estimate the strength of the intermolecular H-bonds.

**NBO Analysis**

The NBO analysis provides an efficient method for studying intermolecular bonding and presents a convenient basis for investigating charge transfer in molecular systems. It is performed using NBO 3.1 program implemented in the Gaussian 03 package using M06-2X/6-311++G(d,p) (see Table 3) and B3LYP/6-311++G(d,p) (see Table S5) levels of theory. Table 3 shows the values of occupation   numbers of
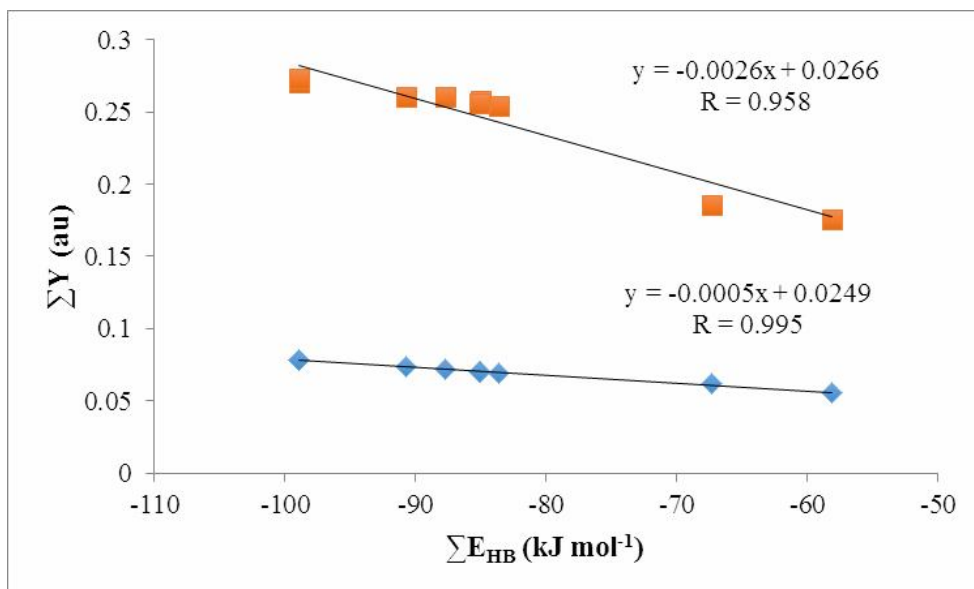
**Fig. 5.** Correlation between sum of the electron density ($\Sigma \rho_{BCP}$ with ♦ sign) and its Laplacian ($\Sigma \nabla^2 \rho_{BCP}$ with ■ sign) at the $O_{VB} \cdots H\text{-}N_U$ and $O(S)_U \cdots H\text{-}O_{VB}$ H-bonds ($\Sigma Y$) *versus* sum of the H-bond energies ($\Sigma E_{HB}$) at the M06-2X/6-311++G(d,p) level of theory.



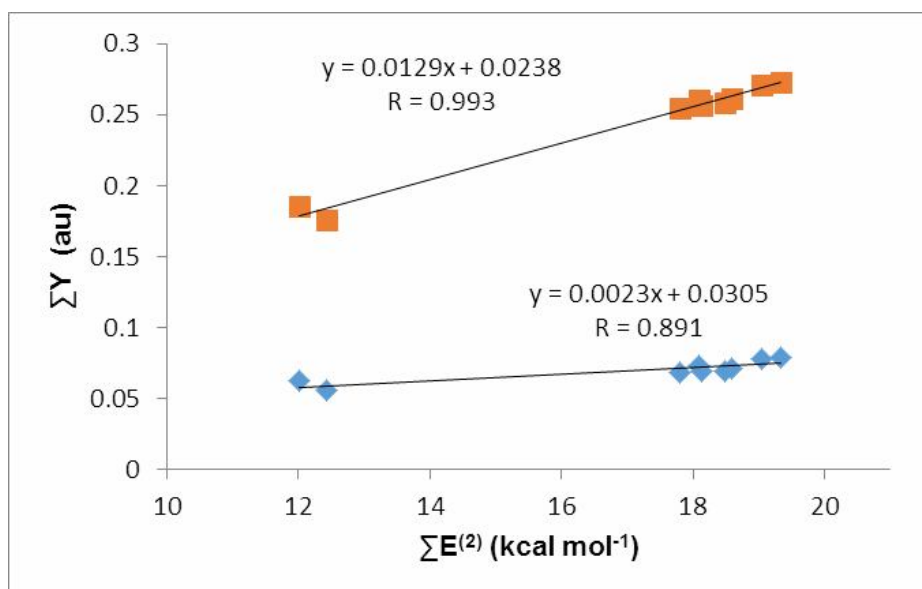**Fig. 6.** Correlation between sum of the electron density ($\Sigma \rho_{BCP}$ with ♦ sign) and its Laplacian ($\Sigma \nabla^2 \rho_{BCP}$ with ■ sign) at the $O_{VB} \cdots H\text{-}N_U$ and $O(S)_U \cdots H\text{-}O_{VB}$ H-bonds ($\Sigma Y$) *versus* sum of the charge transfer energies $E^{(2)}$ ($\Sigma E^{(2)}$) at the M06-2X/6-311++G(d,p) level of theory.

**Table 3.** NBO Analysis of the Formed Complexes Including Occupation Numbers of Donor ($O.N._D$) and Acceptor ($O.N._A$) Orbitals and their Energies (in kcal mol$^{-1}$) Calculated at the M06-2X/6- 311++G(d,p) Level of Theory

|        | LPO$_{VB}$ → σ*N-H$_U$ | | | LPO(S)$_U$ → σ*O-H$_{VB}$ | | |
|--------|--------|--------|--------|--------|--------|--------|
|        | $O.N._D$ | $O.N._A$ | $E^{(2)}$ | $O.N._D$ | $O.N._A$ | $E^{(2)}$ |
| U-VB1  | 1.9652 | 0.0426 | 8.15 | 1.9592 | 0.0585 | 10.89 |
| U-VB2  | 1.9667 | 0.0372 | 7.62 | 1.9612 | 0.0492 | 10.19 |
| U-VB3  | 1.9997 | 0.0398 | 7.87 | 1.9594 | 0.0557 | 10.22 |
| FU-VB1 | 1.9636 | 0.0453 | 8.99 | 1.9603 | 0.0557 | 10.34 |
| FU-VB2 | 1.9654 | 0.0397 | 8.32 | 1.9614 | 0.0481 | 10.17 |
| FU-VB3 | 1.9657 | 0.0395 | 8.08 | 1.9624 | 0.0501 | 10.05 |
| TU-VB1 | 1.9627 | 0.0511 | 9.14 | 1.9779 | 0.0754 | 2.88 |
| TU-VB2 | 1.9631 | 0.0455 | 9.49 | 1.9774 | 0.0634 | 2.94 |
| TU-VB3 | 1.9642 | 0.0452 | 8.86 | 1.9609 | 0.0507 | 9.74 |

N(O)-H anti-bonding orbitals (σ*N(O)-H) and the lone pair electrons of O and S atoms (LPO(S)) and their stabilizing energies ($E^{(2)}$). In the NBO analysis of H-bonded systems, the most important charge transfer occurs between the lone pairs of proton acceptor and anti-bonding orbitals of the proton donor. The theoretical results show that two lone pair electrons of oxygen (or sulfur) atoms act as donor and the σ*N(O)-H anti-bonding orbitals act as acceptor. It is obvious from Table 3 that the most significant donor–acceptor interactions in the studied complexes are the LPO$_{VB}$ → σ*N-H$_U$ and LPO(S)$_U$ → σ*O-H$_{VB}$. As can be observed from this Table, in most cases, the LPO(S)$_U$ → σ*O-H$_{VB}$ interaction demonstrates the higher changes in O(S)$_U$···H-O$_{VB}$ donor-acceptor energies ($E^{(2)}$) with respect to LPO$_{VB}$ → σ*N-H$_U$ interaction.

Our DFT calculations also indicate that the occupancies of σ*O-H anti-bonding orbitals are in the range of 0.0481-0.0754 e and σ*N-H$_{(U)}$ ones lie in the ranges of 0.0372 to 0.0511 e. This clearly shows that the occupancy of σ*O-H$_{(VB)}$ anti-bonding orbitals is larger than the σ*N-H$_{(U)}$ ones. The results also reveal that increase in the occupancy of the σ*N(O)-H anti-bonding orbitals is accompanied with

lengthening of the N(O)-H proton donating bonds and the weakening of these bonds. These results are the strongest evidence of H-bonding formation (see Tables S1 and 3). The results collected in Table 3 also demonstrate that, in most cases, the charge transfer energies ($E^{(2)}$) and the σ*N(O)-H occupancies corresponding to the O$_{VB}$···H-N$_U$ and O(S)$_U$···H-O$_{VB}$ interactions for the U-VB1, FU-VB1 and TU-VB1 complexes are greater than those in the other complexes, which is in agreement with their H-bond energies ($E_{HB}$). In addition, the sum of the charge transfer energies ($\Sigma E^{(2)}$) for the FU-VB1 complex is the greatest with respect to the others. Therefore, these results also confirm that the H-bond in FU-VB1 is stronger than that in the other complexes.

Several correlations between topological and energetic parameters are also found. As shown in Fig. 6, there is a good correlation between the sum of electron densities ($\Sigma\rho_{BCP}$) and their Laplacian ($\Sigma\nabla^2\rho_{BCP}$) versus the sum of charge transfer energies ($\Sigma E^{(2)}$); The correlation coefficients are equal to 0.891 and 0.993, respectively. Figure S3 in the supplementary section, also shows this correlation using B3LYP/6-311++G(d,p) method. The results show a better

correlation for these parameters when B3LYP is used instead of M06-2X method (see Table S5 for more details). Furthermore, the results presented in Tables 1 and 3 indicate a linear relationship between the sum of H-bond energies ($\Sigma E_{HB}$) and the sum of calculated NBO energies ($\Sigma E^{(2)}$) with an excellent correlation coefficient (R is equal to 0.932). Therefore, $\Sigma E_{HB}$ could be easily computed from $\Sigma E^{(2)}$ as follows:

$$\Sigma E_{HB} = -4.4729 \ (\Sigma E^{(2)}) - 7.4581$$

This means that the properties of the charge transfer between the lone pairs of proton acceptor and anti-bonding orbitals of proton donor could be very useful in estimating the H-bond strength. These kinds of correlations are important, because they allow to probe quantitatively the strength of such interactions providing a physical explanation for the process.

## HOMO-LUMO Analysis

The HOMO and LUMO energies and energy gap ($\Delta E_{H-L}$) of the studied systems at the M06-2X and B3LYP levels of theory are given in Tables 4 and S6, respectively. HOMO could act as electron donor, therefore, its energy is related to ionization potential. On the other hand, LUMO could act as electron acceptor, thus, the electron affinity of system depends on LUMO energy. The energy gap between HOMO and LUMO is a sign of stability and chemical reactivity of the molecule [48]. A high energy gap shows more chemical stability and less chemical reactivity of the molecule. The frontier orbitals are drawn to understand the bonding scheme of FU-VB1 complex. The positive phase is red and the negative one is green. Figure 7 reveals that in the titled complex, the HOMO is localized on 5FU fragment, while LUMO is confined by the VB3 fragment. Moreover, the HOMO of the FU-VB1 complex shows anti-bonding character at N-H bond.

Density functional theory also provides insights into the popular qualitative chemical concepts such as electronic chemical potential ($\mu$) [49], hardness ($\eta$) [50] and electronegativity ($\chi$) [51] ($\chi$ is defined as the negative of $\mu$, as: $\chi = -\mu$). These parameters are calculated using Koopmans' theorem [52], as given below:

$$\eta = \frac{I - A}{2} \tag{1}$$

$$\chi = \frac{I + A}{2} \tag{2}$$

$$\mu = \frac{-(I + A)}{2} \tag{3}$$

where A and I are the electron affinity and ionization potential of the complexes, respectively. The electron affinity and ionization energy can be expressed as $A = -E_{LUMO}$ and $I = -E_{HOMO}$ with the help of HOMO and LUMO orbital energies. It is well known that the chemical hardness is a measure of the resistance of a chemical species to change its electronic configuration, while the electronic chemical potential measures the escaping tendency of an electron cloud. The reciprocal of the hardness is the softness which measures the facility of charge transfer and its association with high polarizability [53].

For each uracil group, the HOMO-LUMO band gap of the U-VB1, FU-VB1 and TU-VB1 complexes displays the lowest energy (see Table 4). In fact, the reduction of energy gap in these complexes is due to their high chemical reactivity. From energy gap between HOMO and LUMO, one can find whether the molecule is hard or soft. Large energy gap is an indication of hard molecule and small energy gap is the sign of soft molecule. The results obtained show the smallest hardness values for the U-VB1, FU-VB1 and TU-VB1 complexes. Therefore, it can be concluded that these complexes are softer than the other ones. The soft molecules are more polarizable than the hard ones because they need small energy for excitation [17]. On the other hand, the electronic chemical potential ($\mu$) is known by the similar behavior to that of hardness. As shown in Table 4, the values of negative electronic chemical potential indicate that all complexes are stable. The result of our calculations demonstrates the smallest electronic chemical potentials calculated for U-VB1 (-4.95 eV), FU-VB1 (-4.98 eV) and TU-VB1 (-4.69 eV) complexes. Also, it is obvious from Table 4 that the U-VB1, FU-VB1 and TU-VB1 complexes possess higher electronegativity value among all complexes. Thus, they are the best electron acceptors. With only a few exceptions for TU-VB1 complex, similar data for the related complexes are obtained when B3LYP/6-311++G(d,p) is
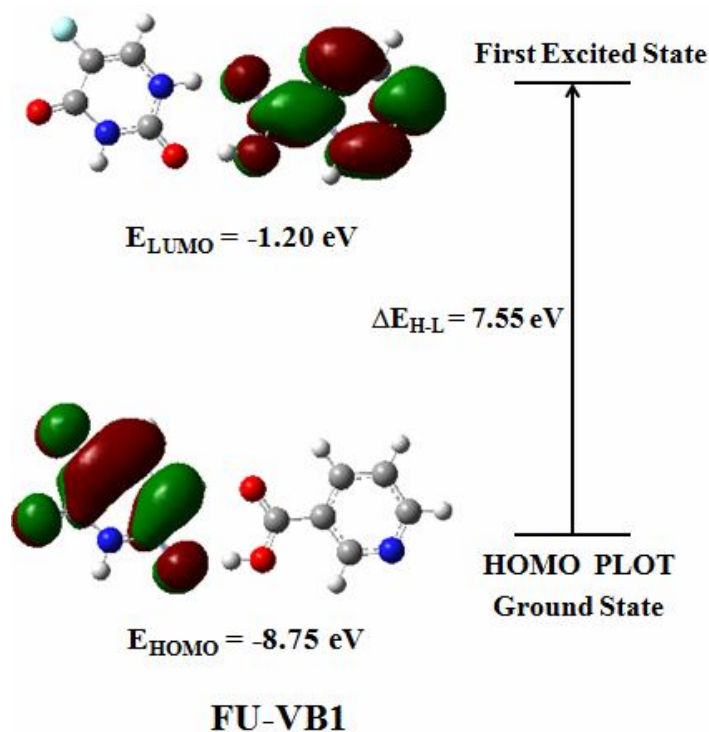
**Fig. 7.** HOMO and LUMO of the FU-VB1 complex obtained at the M06-2X/6-311++G(d,p) level of theory.

**Table 4.** Values of the HOMO and LUMO Energies, the Molecular Orbital Energy Gap ($\Delta E_{H-L}$), Chemical Hardness ($\eta$), Electronic Chemical Potential ($\mu$) and Electronegativity ($\chi$) in Terms of eV Calculated at the M06-2X/6-311++G(d,p) Level of Theory

|        | $E_{HOMO}$ | $E_{LUMO}$ | $\Delta E_{H-L}$ | $\eta$ | $\mu$ | $\chi$ |
|--------|-----------|-----------|---------|--------|--------|--------|
| U-VB1  | -8.789    | -1.115    | 7.673   | 3.837  | -4.952 | 4.952  |
| U-VB2  | -8.856    | -0.891    | 7.966   | 3.983  | -4.873 | 4.873  |
| U-VB3  | -8.834    | -0.903    | 7.931   | 3.965  | -4.869 | 4.869  |
| FU-VB1 | -8.751    | -1.203    | 7.547   | 3.774  | -4.977 | 4.977  |
| FU-VB2 | -8.832    | -0.993    | 7.839   | 3.920  | -4.912 | 4.912  |
| FU-VB3 | -8.776    | -1.081    | 7.695   | 3.847  | -4.929 | 4.929  |
| TU-VB1 | -8.093    | -1.292    | 6.801   | 3.400  | -4.692 | 4.692  |
| TU-VB2 | -8.105    | -1.049    | 7.056   | 3.528  | -4.577 | 4.577  |
| TU-VB3 | -7.933    | -1.082    | 6.851   | 3.426  | -4.507 | 4.507  |

used instead of M06-2X/6-311++G(d,p) method (see Table S6).

## CONCLUSIONS

In this paper, M06-2X/6-311++G(d,p) and B3LYP/6-311++G(d,p) calculations have performed to investigate the H-bond interactions in the formed complexes between VB3 with parent uracil and anticancer uracils (5FU and 2TU). In the studied systems, the uracils could be placed in three preferential interaction sites (A1-A3) in the vicinity of the vitamin B3. Among the various H-bonding sites, the A1 region of uracils showed the strongest interactions, whereas the weakest ones belonged to the A2 region. All complexes had two H-bonds and all of them were found to be planar. The results showed that, in most cases, the H-bonds of the formed complexes are $O_{VB}\cdots H\text{-}N_U$ and $O_U\cdots H\text{-}O_{VB}$, whereas they were different for TU-VB1 and TU-VB2 complexes ($O_{VB}\cdots H\text{-}N_U$ and $S_U\cdots H\text{-}O_{VB}$). It can be also stated that, with only a few exceptions (TU-VB1 and TU-VB2 complexes), the $O(S)_U\cdots H\text{-}O_{VB}$ H-bond distances were shorter than the $O_{VB}\cdots H\text{-}N_U$ ones. Moreover, the calculated topological properties showed that the $O(S)_U\cdots H\text{-}O_{VB}$ interactions have greater values of the electron density with respect to the $O_{VB}\cdots H\text{-}N_U$ ones. Therefore, it could be concluded that the $O(S)_U\cdots H\text{-}O_{VB}$ H-bonds are stronger than the $O_{VB}\cdots H\text{-}N_U$ H-bonds. These results could be also supported by the obtained consequences in the NBO analysis. Furthermore, the DFT calculations and the analyses derived from the AIM and NBO suggested that the most stable and the strongest interactions belonged to the FU-VB1 complex using both methods. The frontier orbital analysis also demonstrated the remarkable role of HOMO-LUMO charge transfer in the stability and chemical reactivity of the studied complexes. Several correlations between topological, geometrical and energetic parameters have been discussed in this article. Therefore, molecular modeling on the complexes formed between VB3 and uracils showed the full ability of the drugs for participating in the formation of a stable intercalation site.

## REFERENCES

[1] P. Hobza, Z. Havlas, Chem. Rev. 100 (2000) 4253.

[2] W. Wang, Y. Zhang, K. Huang, Chem. Phys. Lett. 411 (2005) 439.

[3] A.K. Roy, A.J. Thakkar, Chem. Phys. 312 (2005) 119.

[4] R. Wysokinski, D.C. Biennko, D. Michalska, Th. Zeegers-Huyskens, Chem. Phys. 315 (2005) 17.

[5] A. Ebrahimi, H. Roohi, M. Habibi, M. Mohammadi, R. Vaziri, Chem. Phys. 322 (2006) 289.

[6] A. Ebrahimi, H. Roohi, M. Habibi, M. Hasannejad, Chem. Phys. 327 (2006) 368.

[7] A. Ebrahimi, M. Habibi, H.R. Masoodi, A.R. Gholipour, Chem. Phys. 355 (2009) 67.

[8] H.R. Masoodi, A. Ebrahimi, M. Habibi, Chem. Phys. Lett. 483 (2009) 43.

[9] G.A. Jeffrey, An Introduction to Hydrogen Bonding, Oxford University Press, New York, 1997.

[10] G.R. Desiraju, T. Steiner, The Weak Hydrogen Bond: In Structural Chemistry and Biology, Oxford University Press, USA, 2001.

[11] D. Hadzˇi, Theoretical Treatments of Hydrogen Bonding, John Wiley & Sons, Chichester, 1997.

[12] T. Steiner, Angew. Chem. Int. Ed. 41 (2002) 48.

[13] L. Pauling, The Nature of the Chemical Bond, Ithaca, Cornell University Press, New York, 1960.

[14] G.R. Desiraju, T. Steiner, The Weak Hydrogen Bond in Structural Chemistry and Biology, Oxford University Press, New York, 1999.

[15] M. Małecka, Struct. Chem. 21 (2010) 175.

[16] H. Roohi, A.R. Nowroozi, E. Anjomshoa, Comput. Theor. Chem. 965 (2011) 211.

[17] M. Yoosefian, A. Mola, J. Mol. Liq. 209 (2015) 526.

[18] M. Souri, A. Khan Mohammadi, J. Mol. Liq. 230 (2017) 169.

[19] B. Blicharska, T. Kupka, J. Mol. Struct. 613 (2002) 153.

[20] G.J. Peters, H.H. Backus, S. Freemantle, B. van Triest, G. Codacci-Pisanelli, C.L. van der Wilt, K. Smid, J. Lunec, A.H. Calvert, S. Marsh, H.L. McLeod, E. Bloemena, S. Meijer, G. Jansen, C.J. van Groeningen, H.M. Pinedo, Biochim. Biophys. Acta 1587 (2002) 194.

[21] K.H. Elstein, M.L. Mole, R.W. Setzer, R.M. Zucker, R.J. Kavlock, J.M. Rogers, C. Lau, Toxicol. Appl. Pharmacol. 146 (1997) 29.

[22] K. Ghoshal, S.T. Jacob, Biochem. Pharmacol. 53 (1997) 1569.

[23] E. Ojima, Y. Inoue, H. Watanabe, J. Hiro, Y. Toiyama, C. Miki, M. Kusunoki, Oncol. Rep. 16 (2006) 1085.

[24] M. Malet-Martino, R. Martino, Oncologist 7 (2002) 288.

[25] K.Abdi, Sh. Nafisi, F. Manouchehri, M. Bonsaii, A. Khalaj, J. Photobiol. B: Biology 107 (2012) 20.

[26] A. Shah, E. Nosheen, F. Zafar, S. Noman uddin, D. D. Dionysiou, A. Badshah, Zu. Rehman, G. Shahzada Khan, J. Photochem. Photobiol. B: Biology 117 (2012) 269.

[27] W.B. Baker, J. Pharm. Sci. 34 (1945) 249.

[28] R. Prakash, S. Gandotra, L.K. Singh, B. Das, A. Lakra, Gen. Hospital Psychiatry 30 (2008) 581.

[29] K. Sung-Wook, L. Ju-Hee, M. Ji-Hong, M.D.N. Uddin, L. You-Jin, S. Jae-Won, H. Jin, E. Seong-Kug, L. John-Hwa, P. Sang-Youel, Oncotarget. 7 (2016) 4356.

[30] Institute of Medicine "Niacin". Dietary Reference Intakes for Thiamin, Riboflavin, Niacin, Vitamin B6, Folate, Vitamin B12, Pantothenic Acid, Biotin, and Choline, Washington, DC, The National Academies Press, 1998, pp. 123.

[31] M.J. Frisch, G.W. Trucks, H.B. Schlegel, G.E. Scuseria, M.A. Robb, J.R. Cheeseman, J.A. Montgomery, Jr., T. Vreven, K.N. Kudin, J.C. Burant, J.M. Millam, S.S. Iyengar, J. Tomasi, V. Barone, B. Mennucci, M. Cossi, G. Scalmani, N. Rega, G.A. Petersson, H. Nakatsuji, M. Hada, M. Ehara, K. Toyota, R. Fukuda, J. Hasegawa, M. Ishida, T. Nakajima, Y. Honda, O. Kitao, H. Nakai, M. Klene, X. Li, J.E. Knox, H.P. Hratchian, J.B. Cross, V. Bakken, C. Adamo, J. Jaramillo, R. Gomperts, R.E. Stratmann, O. Yazyev, A.J. Austin, R. Cammi, C. Pomelli, J.W. Ochterski, P.Y. Ayala, K. Morokuma, G. A. Voth, P. Salvador, J.J. Dannenberg, V.G. Zakrzewski, S. Dapprich, A.D. Daniels, M. C. Strain, O. Farkas, D.K. Malick, A.D. Rabuck, K. Raghavachari, J.B. Foresman, J.V. Ortiz, Q. Cui, A.G. Baboul, S. Cli-ord, J. Cioslowski, B.B. Stefanov, G. Liu, A. Liashenko, P. Piskorz, I. Komaromi, R.L.

Martin, D.J. Fox, T. Keith, M.A. Al-Laham, C.Y. Peng, A. Nanayakkara, M. Challacombe, P.M.W. Gill, B. Johnson, W. Chen, M.W. Wong, C. Gonzalez, J.A. Pople, Gaussian 03, Revision A.7, Gaussian, Inc., Pittsburgh, PA, 2003.

[32] S.F. Boys, F. Bernardi, Mol. Phys. 19 (1970) 553.

[33] P. Hobza, R. Zahradnik, Intermolecular Complexes, Elsevier, Amsterdam, 1988.

[34] F.B. van Duijneveldt, J.G.C.M. van Duijneveldt-van de Rijdt, J.H. van Lenthe, Chem. Rev. 94 (1994) 1873.

[35] E. Espinosa, E. Molins, C. Lecomte, J. Chem. Phys. 113 (2000) 5686.

[36] R.F.W. Bader, Atoms in Molecules: A Quantum Theory, Oxford University, New York, 1990.

[37] F. Biegler Ko¨nig, J. Scho¨nbohm, J. Comput. Chem. 23 (2002) 1489.

[38] E.D. Glendening, A.E. Reed, J.E. Carpenter, F. Weinhold, NBO, Version 3.1, Gaussian, Inc., Pittsburgh PA, 1992.

[39] P. Zhou, F. Tian, F. Lv, Z. Shang, Proteins 76 (2009) 151.

[40] J.A. Platts, S.T. Howard, B.R.F. Bracke, J. Am. Chem. Soc. 118 (1996) 2726.

[41] S.J. Grabowski, W.A. Sokalski, E. Dyguda, J. Leszczyn'ski, J. Phys. Chem. B 110 (2006) 6444.

[42] S. Scheiner, Biopolym. 22 (1983) 731.

[43] J. Pranata, S.G. Wierschke, W.L. Jorgensen, J. Am. Chem. Soc. 113 (1991) 2810.

[44] K. Weisz, J. Janhchen, H.H. Limbach, J. Am. Chem. Soc. 119 (1997) 6436.

[45] M.T. Nguyen, A.K. Chandra, T. Zeegers-Huyskens, J. Chem. Soc. Faraday Trans. 94 (1998) 1277.

[46] I. Rozas, I. Alkorta, J. Elguero, J. Am. Chem. Soc. 122 (2000) 11154.

[47] D. Cremer, E. Kraka, Angew. Chem. Int. Ed. Engl. 23 (1984) 627.

[48] P.K. Chattaraj, A. Poddar, J. Phys. Chem. A 103 (1999) 8691.

[49] I. Fleming, Frontier Orbitals: Organic Chemical Reactions, John Wiley and Sons, New York, 1976.

[50] R.G. Pearson, Chemical Hardness, Wiley-VCH,

Oxford, 1997.

[51] K.D. Sen, C.K. Jorgensen, Electronegativity, Structure and Bonding, Springer-Verlag, New York, 1987.

[52] T.A. Koopmans, Physics 1 (1934) 104.

[53] H. Raissi, A. Khanmohammadi, F. Mollania, Bull. Chem. Soc. Jpn. 86 (2013) 1261.